Dun1, a Chk2-related kinase, is the central regulator of securin-separase dynamics during DNA damage signaling

Candice Qiu Xia Yam[1,2], David Boy Chia[3], Idina Shi[1], Hong Hwa Lim[1,2,*] and Uttam Surana ⬤[1,3,2,4,*]

[1]Institute of Molecular and Cell Biology, Agency for Science, Technology and Research (A*STAR), Proteos, 61 Biopolis Drive, Singapore, [2]Bioprocessing Technology Institute, A*STAR, Singapore, [3]Biotransformation Innovation Platform, A*STAR, Singapore and [4]Department of Pharmacology, National University of Singapore, Singapore

ABSTRACT

The DNA damage checkpoint halts cell cycle progression in G2 in response to genotoxic insults. Central to the execution of cell cycle arrest is the checkpoint-induced stabilization of securin-separase complex (yeast Pds1-Esp1). The checkpoint kinases Chk1 and Chk2 (yeast Chk1 and Rad53) are thought to critically contribute to the stability of securin-separase complex by phosphorylation of securin, rendering it resistant to proteolytic destruction by the anaphase promoting complex (APC). Dun1, a Rad53 paralog related to Chk2, is also essential for checkpoint-imposed arrest. Dun1 is required for the DNA damage-induced transcription of DNA repair genes; however, its role in the execution of cell cycle arrest remains unknown. Here, we show that Dun1's role in checkpoint arrest is independent of its involvement in the transcription of repair genes. Instead, Dun1 is necessary to prevent Pds1 destruction during DNA damage in that the Dun1-deficient cells degrade Pds1, escape G2 arrest and undergo mitosis despite the presence of checkpoint-active Chk1 and Rad53. Interestingly, proteolytic degradation of Pds1 in the absence of Dun1 is mediated not by APC but by the HECT domain-containing E3 ligase Rsp5. Our results suggest a regulatory scheme in which Dun1 prevents chromosome segregation during DNA damage by inhibiting Rsp5-mediated proteolytic degradation of securin Pds1.

INTRODUCTION

Cells are constantly exposed to genotoxic stresses during their lifetime, of which a double strand break (DSB) is the most detrimental to cells' subsequent survival (1). If left unrepaired, DNA damage can promote spurious repairs, introducing deleterious genetic mutations and alterations in cells' physiological fate (2,3). To mitigate such consequences, cells activate the DNA damage response (DDR), a concerted cellular response that triggers a network of interacting pathways to efficiently detect the genomic damage, arrest cells' progression through the cell cycle and initiate the repair process (4,5). Genetic instability resulting from the mutations in the DDR genes is a key feature in both cancer and genetic diseases such as Ataxia-telangiectasia that increases disposition to cancer (6,7). The regulatory framework of DDR is largely conserved across eukaryotic organisms and has been extensively studied in both yeast and mammalian cells.

In yeast *Saccharomyces cerevisiae*, the DNA lesions are recognized by the sensors (Ddc1–Rad17–Mec3–Rad24 complex), which in turn activate the upstream effectors of the checkpoint cascade, the phosphatidylinositol 3-kinase like kinases Mec1 and Tel1 (mammalian ATM and ATR) (8,9). An early event in checkpoint activation is the Mec1 dependent phosphorylation of its binding partner Ddc2 (10). Mec1 also targets 9–1–1 complex (a heterotrimeric complex of Rad17, Mec3 and Ddc1), Rad9 and histone H2A. Termed mediator, Rad9 plays a critical role in the recruitment and activation of the downstream effector kinases Chk1 and Rad53 (11). Phosphorylation of Rad53 is a key event in this regulatory cascade and is used as a marker to monitor the activation status of the checkpoint. Transient suspension of cell cycle progression following DNA damage is a critical feature of DDR and is executed by the DNA damage checkpoint. In mammalian cells, DDR accomplishes this task by maintaining the inhibitory phosphorylation on Cdk1 by wee1 and Myt1 kinases (12). Genetic evidence suggest that inhibition of Cdk1 is also aided by the inactivation and translocation of Cdc25C phosphatase

*To whom correspondence should be addressed. Tel: +65 65869503; Fax: +65 67791117; Email: mcbucs@imcb.a-star.edu.sg
Correspondence may also be addressed to Hong Hwa Lim. Tel: +65 65869752; Fax: +65 67791117; Email: lim_hong_hwa@bti.a-star.edu.sg

into the cytoplasm, partly mediated by Ser216 phosphorylation ([13]). In *S. cerevisiae*, the checkpoint imposes mitotic arrest predominantly by targeting the chromosome segregation machinery. During normal mitosis, separation of sister chromatids is initiated by the separase (yeast Esp1) mediated proteolytic cleavage of the Scc1 subunit of the cohesion complex that tethers sister chromatids to each other until the metaphase-to-anaphase transition. Prior to the onset of anaphase, Pds1 (yeast securin) binds to Esp1 and inhibits its activity, thus precluding premature transition to anaphase ([14–17]). At the end of metaphase, Cdc20-activated E3 ligase APC (APC^{Cdc20}) catalyses the proteolytic destruction of Pds1, thus freeing Esp1 from the inhibitory constraint to initiate cohesin cleavage ([18,19]). Although APC^{Cdc20} remains active in pre-anaphase arrested cells following DNA damage ([20]), it has been proposed that Pds1 phosphorylation by Chk1 kinase (and possibly Rad53) is a key step in preventing anaphase onset. Collectively, these findings imply that phosphorylation of Pds1 renders it resistant to APC^{Cdc20} mediated proteolytic degradation, resulting in the stabilization of Pds1-Esp1 complex and inhibition of chromosome segregation. Once DNA damage is repaired and checkpoint is extinguished, it is imperative that phosphorylated Pds1 be either dephosphorylated and 're-sensitized' to APC-mediated proteolysis or undergo degradation catalysed by another E3 ligase to allow chromosome segregation. No specific phosphatase or E3 ligase for phosphorylated Pds1 has been reported thus far.

Dun1, a kinase structurally and functionally related to Rad53, is also implicated in DDR. It was identified in a screen for genes involved in DNA damage-induced transcription of *RNR3*, a subunit of ribonucleotide reductase ([17]). During normal division cycle, transcription factor Rfx1/Crt1 represses transcription of multiple genes involved in the damage-induced regulation of nucleotide synthesis or DNA repair such as *RNR2*, *RNR3*, *RNR4* and *HUG1*. Upon DNA damage, this transcription repression is relieved by hyper-phosphorylation of Rfx1 by Dun1. Dun1 also directly phosphorylates Sml1, an inhibitor of RNR which undergoes degradation upon DNA damage ([21–23]). Thus, Dun1 plays important roles in the switching on of repair genes and regulation of dNTP levels in response to DNA damage. Both Rad53 and Dun1 contain Forkhead-associated (FHA) domains important for their activation in response to DNA damage. Rad53, but not Dun1, also contain two SQ/TQ cluster domains (SCD1 and SCD2) which are phosphorylated by Mec1. Phosphorylated SCD1 of Rad53 can bind to Dun1's FHA domain to promote its phosphorylation-dependent activation ([24]).

Dun1's role in DDR is not restricted only to DNA damage-induced transcription. Indeed, Dun1 mutants were found to be defective in G2 arrest following DNA damage, suggesting that it is also involved in the execution of the damage-induced cell cycle arrest ([25,26]). Previous studies have suggested two parallel pathways for the execution of checkpoint arrest: one emanating from Rad53/Dun1; the other dependent on Chk1-Pds1 axis ([27]). It is puzzling that *dun1Δ* cells which are *CHK1* and *RAD53* proficient fail to mount a G2 arrest in response to DNA damage. While the regulation of repair genes and damage-dependent dNTP synthesis are well-established roles of Dun1, molecular event(s) that Dun1 modulates during execution of G2 arrest is not clear. In this study, we have investigated the involvement of Dun1 in the damage-induced inhibition of mitotic progression. We find that *dun1Δ* cells fail to inhibit the onset of mitosis despite the presence of checkpoint-activated Chk1 and Rad53, suggesting that Dun1 kinase is a critical effector in the execution of cell cycle arrest. *dun1Δ* cells exhibit diminished Esp1-Pds1 association, degrade Pds1 and undergo anaphase. Surprisingly, Pds1 proteolysis in *dun1Δ* cells is not dependent on APC but on HECT domain containing E3 ubiquitin ligase Rsp5. Thus, E3 ligase Rsp5 is an important player in DNA damage signalling. Based on our observations, we propose that Dun1 imposes cell cycle arrest by stabilizing Pds1-Esp1 complex via inhibition of Rsp5-mediated proteolytic degradation of Pds1.

MATERIALS AND METHODS

Yeast strains, culture conditions and reagents

All strains used in this study were derivatives of JKM139 ([28,29]), unless mentioned otherwise (Supplemental Table S1). Standard molecular genetics and molecular biology techniques were used to construct plasmids and strains of various genotypes. PCR-based genotyping was used to confirm gene disruptions and gene replacements. Cells were routinely cultured in Yeast Extract Peptone medium (YEP: 1.1% yeast extract, 2.2% peptone, 50 ml/l adenine) supplemented with 2% glucose or raffinose + galactose.

For over-expression of Rfx1 (US8005) and Chk1 (US8267), *RFX1* or *CHK1* gene was tagged with HA$_9$ epitope at the 5' end, and cloned under the control of *GAL1* promoter. The resultant plasmid was linearized and stably integrated at the *TRP1* locus. Ddc2 was tagged with Citrine at the C-terminus using the one-step tagging method as described ([30]). To investigate securin dynamics, endogenous *PDS1* (securin) was tagged with HA$_3$ epitope using *URA3*-based pOC52 construct (a gift from Prof. Orna Cohen-Fix, National Institutes of Health). To generate TEV protease-sensitive, conditional ESP1 mutant (*mESP1*), a construct (pUS2178) containing TEV proteinase under the control of *GAL1* promoter at the *TRP1* locus. The endogenous *ESP1* gene was then replaced with *mESP1*, in which the sequence between 548–554 aa was modified into TEV proteinase cleavage sequence ENLYFQG by Quik mutagenesis (Agilent, 200522). To introduce the *rsp5-1* mutation into the JKM179 derived yeast strains, the temperature sensitive mutation (L733S) containing fragment was amplified from the *rsp5-1* strain FW1808 (Prof Fred Winston, Harvard Medical School). Gibson tagging method (New England Biolabs, E2611L) was employed using 1458 bp of *rsp5-1* gene sequence, *TRP1* cassette (selection marker) and 3' UTR of *RSP5* to generate pUS4400 which was then digested with Kpn1/EcoRI and this fragment was used to replace the endogenous *RSP5*. Complete strain list is in Supplemental Table S1.

Synchronization of cells and activation of checkpoint

Briefly, yeast cells were synchronized in G1 by α factor treatment (1 μg/ml for *bar*Δ strains or 5 μg/ml BAR+ strains)

in YEP medium supplemented with 4% raffinose. After incubation for 2 h, α factor was removed and cells were released into YEP + raff + gal medium to induce HO endonuclease expression from *GAL1* promoter. HO expression introduces DNA damage in form of an unrepairable double strand break at the *MAT* locus, allowing sustained activation of the DNA damage checkpoint. In most cases, cells also harboured *slk19Δ* and *cdc15-2* mutations. At 30°C, these mutations constituted a telophase trap, preventing mitotic progression beyond telophase. In all experiments, a water-bath was used to incubate the strains at the required temperatures. To accommodate the slight temperature fluctuation (within 1°C) in the water-bath, the temperature was set at 31°C instead of 30°C to effectively activate the telophase trap. In the experiments involving temperature sensitive mutations *cdc23-1* and *rsp5-1*, G1 synchronized cells at 24°C were allowed to resume cell cycle progression at 37°C to inactivate the corresponding protein. In the experiments involving DNA damage in mitotic cells, G1 synchronized cells were released into medium containing Nocodazole for 2 h and treated with MMS (0.025%) for 30 min. Nocodazole was then removed and cells were released into fresh medium in the absence or presence of MMS as required. Cell samples were collected at different time intervals for analyses. All experiments in this study were repeated at least three times (triplicates) using the same strain (strain numbers are mentioned in the figure legends and their genotypes are listed in Supplementary Table S1). All experimental conditions and the strains were identical in the triplicate experiments.

Quantitative real-time PCR

To prepare samples for RNA extraction, an equal volume of ice was added immediately after cells were collected, followed by ice-cold 1xPBS wash before storing them at –20°C. To extract mRNA, an equal volume of acid-washed glass beads was added to the cell pellet, followed by 300 μl each of RNA Cross Buffer (0.3 M NaCl, 10 mM Tris pH7.5, 1 mM EDTA and 0.2% SDS) and phenol–chloroform solution. Cells were lysed by mechanical agitation at full speed at 4°C for 10 min and the lysates were centrifuged at 4°C to separate the nucleic acids from the cell debris. The nucleic acid suspension was stored in ice-cold ethanol. To preserve only the mRNA, these suspensions were digested using DNase kit (Turbo DNA-free, Invitrogen). 2 μM of RNA preparation from each sample was used to perform RT-PCR (RevertAid, Thermo Scientific), resulting in 20 μl of cDNA solution each. Quantitative PCR was carried out using the Bio-Rad CFX Connect Real Time system. Each PCR consisted of: 10 μl reaction containing 2 μl of cDNA sample, 0.05 μl of each Forward and Reverse Primers (100μM) to detect *HUG1/RNR3* and 5 μl of 2× Sybr Green KAPA Biosystem KK4608. The following primers were used to detect *HUG1*, *RNR3* and *G6PDH* expression:

For *HUG1* (detection of 183 bp fragment): OUS6321 - 'TTAACCCAAAGCAATTCT TCCTTG' and OUS6322 'TGGAAGTATTCTTACCAATGTCAG'. For RNR3 (to detect 207 bp fragment): OUS6319 - 'TGCTGATCGTGC CATCTACATC' and OUS6320 'ATATGTGTAGCGGC

TTGATCGG'. For G6PDH (to detect 242 bp fragment, as a control): OUS7078 - 'CGTGGATGATGACACTGT AGAC' and OUS7079 – 'ACTTTAGGTACACAGCGG CATC'.

The qPCR program was carried out on a Bio-Rad CFX connect Real time system using 60°C annealing temperature with 40 s of extension time for each PCR cycle. For qPCR, experiments for each strain were performed in triplicates (referred to as three sets). For each set, qPCR reaction on each RNA sample was performed in triplicates. Each sample was normalized against its own internal control (*G6PDH*), as in Figure 2B. In experiments where samples were analysed at different time-points, the results are normalized against its own internal control (*G6PDH*) and the fold-change in gene expression was calculated by taking expression in the 1 h sample as the baseline (as in Figure 2D).

Bimolecular fluorescence complementation (BiFC) assay and flow cytometry

To generate *ESP1* with C-terminally tagged VC (first half of Venus protein), the last 1051 bp of *ESP1* gene just before the stop codon was inserted between the Sma1 and Sal1 sites of pFA6a-*VC-TRP1* (31). The resultant plasmid pFA6a-*ESP1-VC-TRP1* (pUS3781) was linearized and integrated into the endogenous *ESP1* locus. In the same strain, Pds1 was similarly N-terminally tagged with VN (second half of Venus protein) and expressed from its native promoter. In order to achieve unbiased scoring, cell counts were performed on samples identified only by their strain numbers. Strain numbers were matched with their genotypes only after the consolidation of count-results. In the 'synchronization and release' experimental regime, cells were harvested at different time points and fixed overnight in 70% ethanol. Ethanol was removed and samples were incubated with 0.1% RNase A in 0.2 M Tris–HCl pH7.5, 20 mM EDTA at 37°C for 4 h. RNase A was removed and samples were resuspended in 0.1 ml Propidium iodide solution (50 mg/ml in PBS), sonicated for 5 s before analysis to remove any clumping and were analyzed using the BD FACSCalibur machine. For each sample, 20,000 cells were counted. The histograms were plotted using the WinMDI software (Purdue University Cytometry Laboratories).

Protein extraction, Western blotting and immunoprecipitation

Cells harvested at specific time points were washed with STOP-MIX (0.9% NaCl, 1 mM NaN3, 10 mM EDTA, 50 mM NaF) and stored as pellets at –20°C. For Western blotting, cell pellets were resuspended in YEX (1.85 M NaOH, 7.5% β-mercaptoethanol) lysis buffer, followed by addition of 50% trichloroacetic acid. Protein pellets were collected and resuspended in 100 μl SDS gel-loading buffer. Proteins samples were separated on 10% (29:1) gels. For detection of Pds1-HA$_3$, samples were resolved on 10% 30:0.2 acrylamide:bis-acrylamide gels. Nitrocellulose membranes (GE Healthcare, 10600016) were probed with either primary rabbit polyclonal anti-HA (Sigma Aldrich) to detect Rad53-HA$_2$ or mouse polyclonal F7 anti-HA (Santa

Cruz) to probe Pds1-HA$_3$. For all MYC tagged proteins, primary mouse monoclonal 9E10 anti-MYC (Santa Cruz) was used and rabbit anti-G6PDH (Sigma Aldrich) was used to probe the loading control G6PDH. For Co-IP, cell pellets were thawed in ice-cold NP40 lysis buffer, mixed with the same volume of acid-washed glass beads and disrupted using mechanical agitation at 4°C. Cell lysate was collected by removing the cell debris and beads by centrifugation at 15,000 rpm for 15 min in 4°C. For immunoprecipitation, 0.5 mg equivalent of protein lysate was mixed with rabbit polyclonal anti-HA antibody-conjugated beads (Y-11, sc-805, Santa Cruz Biotechnology) or rabbit polyclonal anti-MYC antibody-conjugated beads (A-14, sc-789, Santa Cruz Biotechnology). These suspensions were incubated for at least 6 h at 4°C and then washed 5× with cold lysis buffer. 5× gel loading buffer was added to the beads and the suspensions were incubated at 100°C for 5 min. The agarose beads were removed by centrifugation and the samples were resolved on 10% polyacrylamide gels.

Quantifying Western blot signals

Quantifications of the relative intensities of protein bands were performed using the gel analysis method in ImageJ program (http://rsb.info.nih.gov/ij/index.html). Briefly, the area of each band of interest is highlighted and displayed as a profile plot. The area under the curve represents the relative intensity value of the band of interest against the loading control (G6PDH) band of an identical size. All experiments for these analyses are repeated at least three times (triplicates). The triplicates were performed with identical strains and experimental conditions. The average relative intensity value of each protein band of interest is reported with its standard deviation, representing the variation over the triplicate experiments.

Immunofluorescence microscopy

Cells samples were fixed overnight in 1 ml KPF (0.1 M KH$_2$PO$_4$ pH6.4, 3.7% formaldehyde), then washed and digested for 1 h in SBC buffer (1.2 M sorbitol, 0.1 M KH$_2$PO$_4$, pH 5.9, 0.7% citric acid) containing 20 μl Glusulase (Perkin Elmer, NEE154001EA) and 5 μl 10 mg/ml lyticase. Digested cells were placed on poly-L-lysine coated glass slides, immune-stained with rat monoclonal anti-tubulin YOL1/34 (Serotec) and mounted in Vectashield containing DAPI (Vector Laboratories) for visualization of mitotic spindles and the nuclei, respectively. For in vivo imaging of Ddc2-Citrine tagged cells and cells containing N-terminal half-Venus-Pds1 and Esp1-Venus-C-terminal half, cells were washed once with PBS and resuspended in 5 μl of Vectashield before imaging. Images were captured with Plan Apochromat 100X objective of the Zeiss Axiolmager motorized microscope equipped with EXFO 120 W metal halide illuminator and a Photometrics CoolSNAP HQ2 high sensitivity monochrome camera. The microscope is driven by the Metamorph software (Universal imaging Corporation).

RESULTS

Dun1 deficient cells are unable to impose G2/M in response to DNA damage

To study the effect of Dun1 deficiency on damage-induced checkpoint arrest, we used a modified version of the yeast strain JKM179 (generously provided by Dr James Haber). JKM179 strain carries deletions of *HML* and *HMR* loci and expresses HO endonuclease under the control of *GAL1* promoter (28,29). When grown in presence of galactose, this strain expresses HO and incurs a single, non-repairable double-strand break at *MAT* locus, leading to the activation of DNA damage checkpoint and subsequently, G2 arrest. To this strain, we added a 'telophase trap' by introducing *slk19Δ* and *cdc15-2* mutations that conditionally inactivate both FEAR (Cdc Fourteen Early Anaphase Release) and MEN (Mitotic Exit Network) pathways at 31°C and preclude mitotic exit. Under conditions which permit this strain (US5750) to overcome G2 arrest, the presence of telophase trap would allow a quantitative measure of the fraction of cell population escaping the arrest. Almost all strains constructed for this study (unless mentioned otherwise) are derived from the modification of JKM179.

 DUN1 and its *dun1Δ* version were synchronized in G1 by α factor treatment, released into raff+gal medium at 31°C and analyzed at different time intervals for DNA content, the status of mitotic spindle and the nucleus, and the activation of DNA damage checkpoint indicated by Chk1 and Rad53 phosphorylation. We monitored the cells only until 8 h to avoid initiation of adaptive response to DNA damage. *DUN1* cells arrested in G2 with a dumbell shaped morphology, short mitotic spindle, an undivided nucleus, 2N DNA content (Figure 1A, B) and phosphorylated Chk1 and Rad53, indicating that checkpoint has been activated (Figure 1C). Rad53 phosphorylation declined at 8 h, perhaps as cells prepared to undergo adaptation. ~60% of *dun1Δ* failed to arrest in G2; they entered mitosis beginning at 4 h and eventually arrested at telophase (due to telophase trap) with long spindle and 2N DNA content (Figure 1A, B). Interestingly, though somewhat lower than in the *DUN1* cells, *dun1Δ* cells exhibited substantial phosphorylation of both Chk1 and Rad53 (Figure 1C), suggesting that *dun1Δ* cells can sense DNA damage and activate the checkpoint but yet progress through mitosis with fully functional checkpoint. These results also imply that checkpoint-activated Chk1 and Rad53 are unable to prevent onset of mitosis in the absence of Dun1 and that Dun1 is perhaps an important element in the execution of checkpoint-induced G2 arrest.

Role of Dun1 in checkpoint-induced arrest is independent of its function in transcription regulation

The role of Dun1 kinase in the upregulation of DNA repair related genes during DNA damage response is well established (17,22). Mec1–Rad53–Dun1 axis participates in the transcriptional upregulation of DNA damage-inducible genes such as *HUG1* and *RNR3* by inhibition of transcription repressor Rfx1 via phosphorylation. Deletion of *DUN1* suppressed *HUG1* and *RNR3* expression during DNA damage while depletion of *RFX1* resulted in the increased expression of *HUG1* and *RNR3* (Supplementary
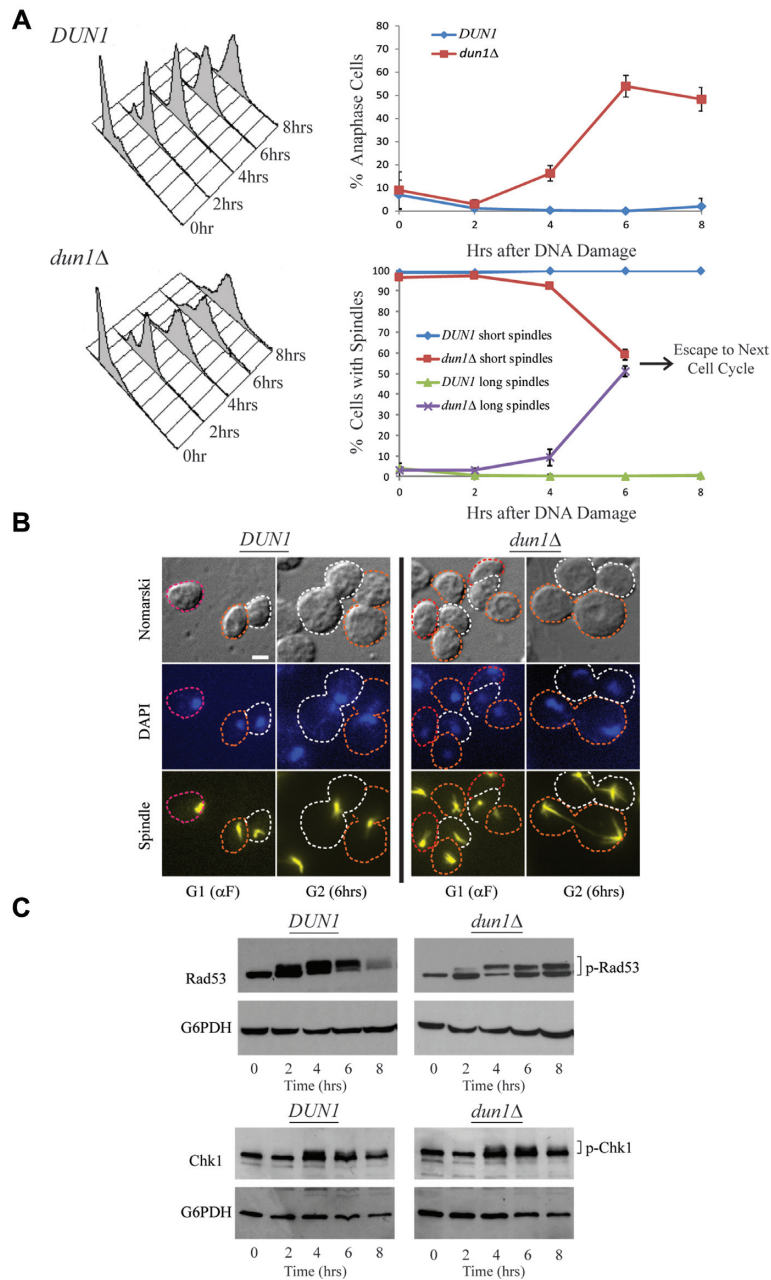
Figure 1. Dun1 deficient cells are unable to arrest in G2 in response to DNA damage. (**A**) *DUN1 RAD53-HA₂* (US7191) and *dun1Δ RAD53-HA₂* (US7192) cells were synchronized in G1 by α factor (0 h timepoint) for 2 h and were then released into YEP+raff+gal medium at 31°C to induce HO-mediated DNA damage. Samples were harvested every 2 h and analysed for nuclear division (DAPI staining), mitotic spindle and DNA content (FACS graph on left). Right (top) graph shows the proportion of cells that had entered anaphase (nuclear division) and right (bottom) graph shows percentage of cells with long and short spindles. Experiments were performed in triplicates (see description in Materials and Methods), 100 cells were counted ($n = 100$) for each timepoint. The error bars on each time-point correspond to the standard deviation of percentage of anaphase cells (right top graph) and percentage of cells with long and short spindles (right bottom graph). (**B**) Photomicrographs of cells at 6 h. Cell morphology, the state of mitotic spindle and the nucleus in both *DUN1* and *dun1Δ* are shown. Individual cells are outlined (scale bar: 5 μm). (**C**) Top panel shows Western blot analysis of Rad53 dynamics in US7191 and US7192 collected from (A), probed using anti-HA antibody. Bottom panel: *DUN1 CHK1-MYC₁₈* (US6317) and *dun1Δ CHK1-MYC₁₈* (US6881) cells were harvested under similar conditions as in (A) and Western blot analyses were performed using anti-myc antibody. G6PDH was used as a loading control.
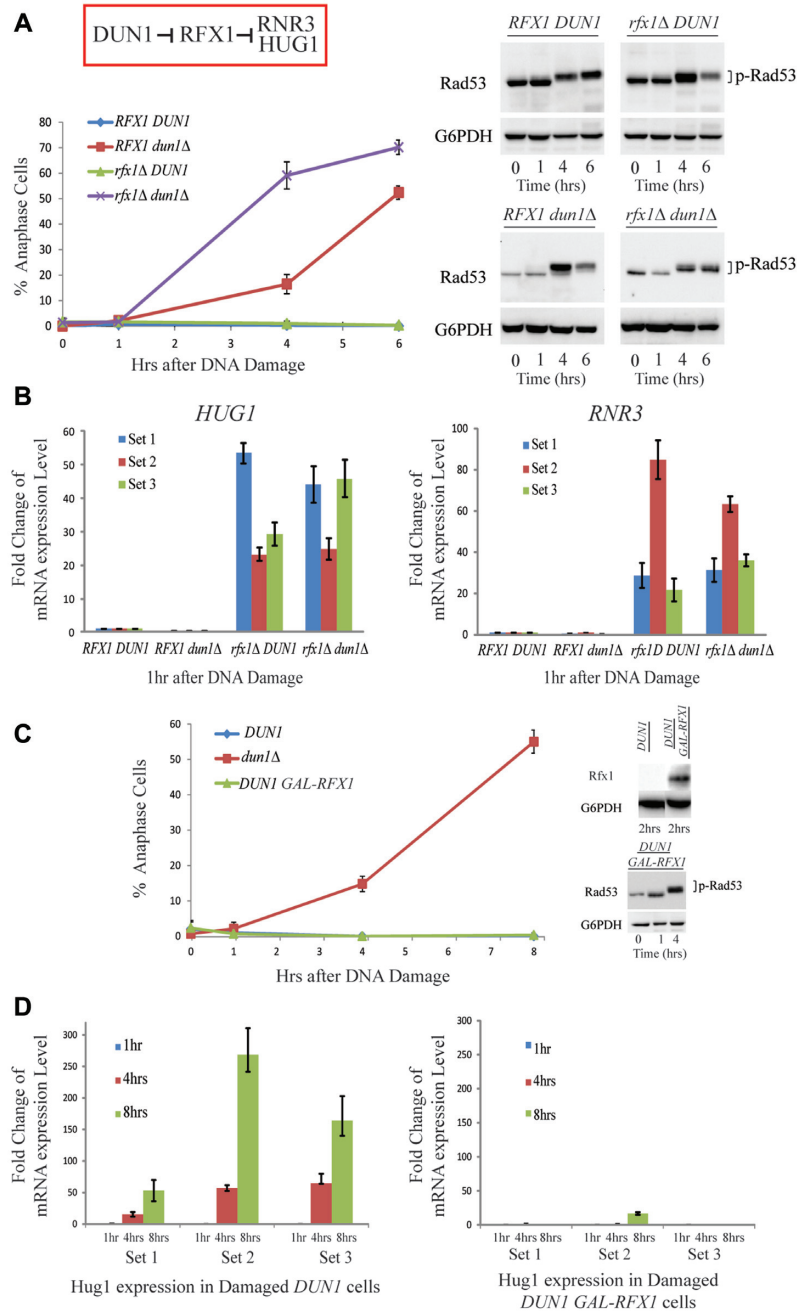
Figure 2. Role of Dun1 in checkpoint-induced arrest is independent of its function in transcriptional regulation. (**A**) Top-left: schematic diagram showing regulatory relationship between *DUN1*, *RFX1* and *RNR3/HUG1*. Lower-left panel: G1 synchronized *RFX1 DUN1* (US7191), *RFX1 dun1Δ* (US6677), *DUN1 rfx1Δ* (US7820) and *dun1Δ rfx1Δ* (US8882) cells containing Rad53-HA$_2$ were released at 31°C in YEP+raff+gal medium to induce HO-mediated DNA damage. At specific time-points, samples were harvested and the number of anaphase cells was quantified by immunofluorescence staining of the spindle. Experiments were performed in triplicates ($n = 100$) and error bars correspond to standard deviation of percentage of anaphase cells. Right panel: Western blot analyses of Rad53, probed using anti-HA antibody at various time-points. (**B**) Quantitative Real-time PCR was performed on samples harvested 1 h after DNA damage was induced in the experiment described in (A). Expression levels of *HUG1* (left) and *RNR3* (right) were normalized to *G6PDH* levels in the respective strains. The analyses were performed in triplicates (sets 1, 2 and 3) (see Materials and Methods for details). Error bars in each set represent standard deviation of fold change in mRNA expression levels of *HUG1* (left) and *RNR3* (right). (**C**) Effect of Rfx1 overexpression on G2 arrest of *DUN1* cells. G1 synchronized *DUN1* RFX1 (US5750), *dun1Δ* RFX1 (US 6677) and *DUN1 GAL-HA₉-RFX1* (US8005) cells were released into YEP+raff+gal medium to induce the expression of *HO* and *RFX1*. The number of cells which had entered anaphase was quantified at various time intervals. Experiments were performed in triplicates ($n = 100$). The error bars correspond to standard deviation of the proportion of anaphase cells at each time-point. Right panel: Western blot showing the overexpression of Rfx1 in US8005 as compared to US5750 2 h after galactose addition. Samples were probed with anti-HA antibody. Western blot showing Rad53 phosphorylation in *DUN1 GAL-HA₉-RFX1* cells at 1 and 4 h after the induction of DNA damage using anti-Rad53 antibody. (**D**) Quantitative Real-time PCR analysis of samples harvested in the experiment described in (C). *HUG1* expression levels in *DUN1* (US5750) and *DUN1 GAL-RFX1* (US8005) were normalized to *G6PDH* levels in the respective strains. Experiments were performed in triplicates (sets 1, 2 and 3) (see Materials and Methods for details). The error bars represent standard deviation of fold change in mRNA expression levels of *HUG1* at each time-point.

Figure S1) (23,32,33). We asked if premature anaphase onset in damaged *dun1Δ* cells is due to a lack of Dun1-directed transcriptional response. Hence, we attempted to compensate for the absence of Dun1-mediated inhibitory phosphorylation of RFX1 in *dun1Δ* strains by deleting *RFX1* gene. *RFX1 DUN1*, *RFX1 dun1Δ*, *rfx1Δ DUN1* and *rfx1Δ dun1Δ* cells were synchronized in G1 by α factor treatment, released in raff+gal medium at 31°C to induce *HO* expression and monitored for their ability to escape G2 arrest. As expected, *RFX1 DUN1* and *rfx1Δ DUN1* cells efficiently arrested in G2, whereas *RFX1 dun1Δ* mutant did not arrest, with >50% cells progressing to anaphase by 6 h (Figure 2A). *rfx1Δ dun1Δ* cells also failed to arrest in G2 with >60% of them entering anaphase at the end of the experiment by 4h, significantly earlier than RFX1 *dun1Δ* cells. Besides Dun1, Rfx1 is also regulated by other molecular factors during genomic stress (34), contributing to the damaged cells' overall arrest response. As such, deletion of Rfx1 together with Dun1 may further alleviate inhibition of cell cycle arrest as compared to *dun1Δ* cells alone, resulting in *rfx1Δ dun1Δ* cells escaping cell cycle arrest earlier than *dun1Δ* cells (Figure 2A).

In all cases, the DNA damage checkpoint was active as indicated by Rad53 phosphorylation (Figure 2A, right panel). We also monitored the expression of damage-inducible genes *HUG1* and *RNR3* by qPCR. Since we found variability in qPCR results for these genes, we conducted the qPCR runs in three sets (see Materials and Methods for details) for both genes. Despite the noticeable variability, *RFX1 DUN1* and *RFX1 dun1Δ* strains showed negligible expression of *HUG1* and *RNR3* genes. In contrast, *rfx1Δ DUN1* and *rfx1Δ dun1Δ* cells consistently exhibited up regulation of both genes (Figure 2B). In a reciprocal experiment, we introduced *GAL-HA₉-RFX1* construct in *DUN1* cells and determined if forced expression of Rfx1 would allow *DUN1* cells to mimic *dun1Δ* cells and escape G2 arrest. G1-synchronized *DUN1, dun1Δ* and *DUN1 GAL-HA₉-RFX1* cells were released into raff+gal medium and monitored for their ability to overcome the cell cycle arrest. As anticipated, *dun1Δ* cells entered anaphase; however, both *DUN1* and *DUN1 GAL-HA₉-RFX1* cells efficiently arrested in G2 (Figure 2C). Consistent with Rfx1's role in transcription repression, *RFX1* expression in *DUN1* cells abolished the damage-induced *HUG1* expression (Figure 2D, right panel). These results imply that Dun1's role in the execution of G2/M arrest is largely unrelated to its role in the inducing transcription in response to DNA damage.

Premature degradation of securin Pds1 in *DUN1* deficient cells

To investigate Dun1's role in promoting G2 arrest upon DNA damage, we tracked relevant indicators in the context of the DNA damage checkpoint such as Ddc2, Cdc5, Pds1 and Scc1. Ddc2 is an upstream checkpoint protein (yeast homolog of human *ATRIP*) which associates with Mec1. The recruitment of Mec1-Ddc2 complex to the DNA damage site is an early event in checkpoint activation (35). Cdc5 is a serine–threonine kinase implicated in adaptation to DNA damage and inhibited by checkpoint kinase Rad53 (36,37). Pds1 (yeast securin) inhibits cohesin

cleaving-enzyme separase (19). Scc1 is a subunit of cohesin complex cleaved by separase during chromosome segregation (38). Although Chk1 and Rad53 are phosphorylated in *dun1Δ* cells upon DNA damage (checkpoint is activated, Figure 1), we also sought to determine the status of the upstream events. The endogenous *DDC2* gene was tagged with Citrine in both *DUN1* and *dun1Δ* strains and G1-synchronized cells were released into raff+gal medium. Ddc2-Citrine was recruited to the damage site (visible as green dots) in progressively increasing proportion in both *DUN1* and *dun1Δ* cells (Figure 3A) indicating that Dun1 deficiency does not affect Ddc2 recruitment. Similarly, Cdc5 kinase remains unaltered in both strains (Figure 3B). In both *DUN1* and *dun1Δ* cells, phosphorylated form of Pds1 appeared at 4 h after DNA damage. However, compared to *DUN1* cells, the phosphorylated form of Pds1 showed visibly lower abundance in *dun1Δ* cells, implying that Pds1 is unstable in absence of Dun1 (Figure 3B, Supplementary Figure S2A). We sought to quantitate Pds1 dynamics in both *DUN1* and *dun1Δ* cells. Using Pds1 total protein levels at 2 h as a standard, the relative fold changes in the intensity of total Pds1 protein levels at 6 and 8 h for *DUN1* cells are 1.49 ± 0.11 and 2 ± 0.33 respectively, reflecting an increase in intensity of Pds1 bands due to DNA-damage dependent phosphorylation and stabilization during cell cycle arrest. In contrast, the relative fold change in the intensity of total Pds1 in *dun1Δ* cells at 6 h remains unchanged as compared to 2 h (0.99 ± 0.29), suggesting a lack of an increase in Pds1 phosphorylation and stabilization. Specifically, the relative fold change in the density of the proportion of phosphorylated Pds1 (upper band) with respect to the total Pds1 levels at 6 h in *DUN1* cells as compared to *dun1Δ* cells is 1.93 ± 0.1, reflecting a lower population of phosphorylated Pds1 in *dun1Δ* cells (Figure 1A, Supplementary Figure S2A). Consistent with these results, Scc1 remained uncleaved in *DUN1* cells as they efficiently arrest in G2, whereas in *dun1Δ* cells, which fail to arrest and undergo anaphase, Scc1 cleavage was seen at 6 h and 8 h. To ensure that anaphase onset in *dun1Δ* is mediated by separase Esp1, we modified Esp1 (mEsp1) in *DUN1* and *dun1Δ* cells such that it contains a TEV cleavage site (ENLYFQG) between 548–554 amino acid residues and also introduced a *GAL-TEV* construct (39). Although mESP1 is fully functional, induced expression of TEV protease cleaves it at the (ENLYFQG) site and renders it non-functional. G1-synchronized cells were released into raff+gal medium to determine if Esp1 inactivation can prevent *dun1Δ* from undergoing anaphase upon DNA damage. Indeed, TEV-mediated inactivation of Esp1 inhibits *dun1Δ* cells from progressing to anaphase (Figure 3C).

We also tested if cohesin complex is destabilised in *dun1Δ* cells, leading to premature chromosome segregation during cell cycle arrest. We increased the stability of cohesin complexes in *dun1Δ* cells: (i) by overexpression of Eco1, an acetyltransferase which promotes association of cohesin complex with sister chromatids and (ii) by deletion of Wpl1 which modulates cohesion establishment (40). We found that both *GAL-HA-ECO1 dun1Δ* cells and *wpl1Δ dun1Δ* cells enter anaphase upon DNA damage with dynamics comparable to that of *dun1Δ*, suggesting that cohesion ring formation and stability are not major contributing factors
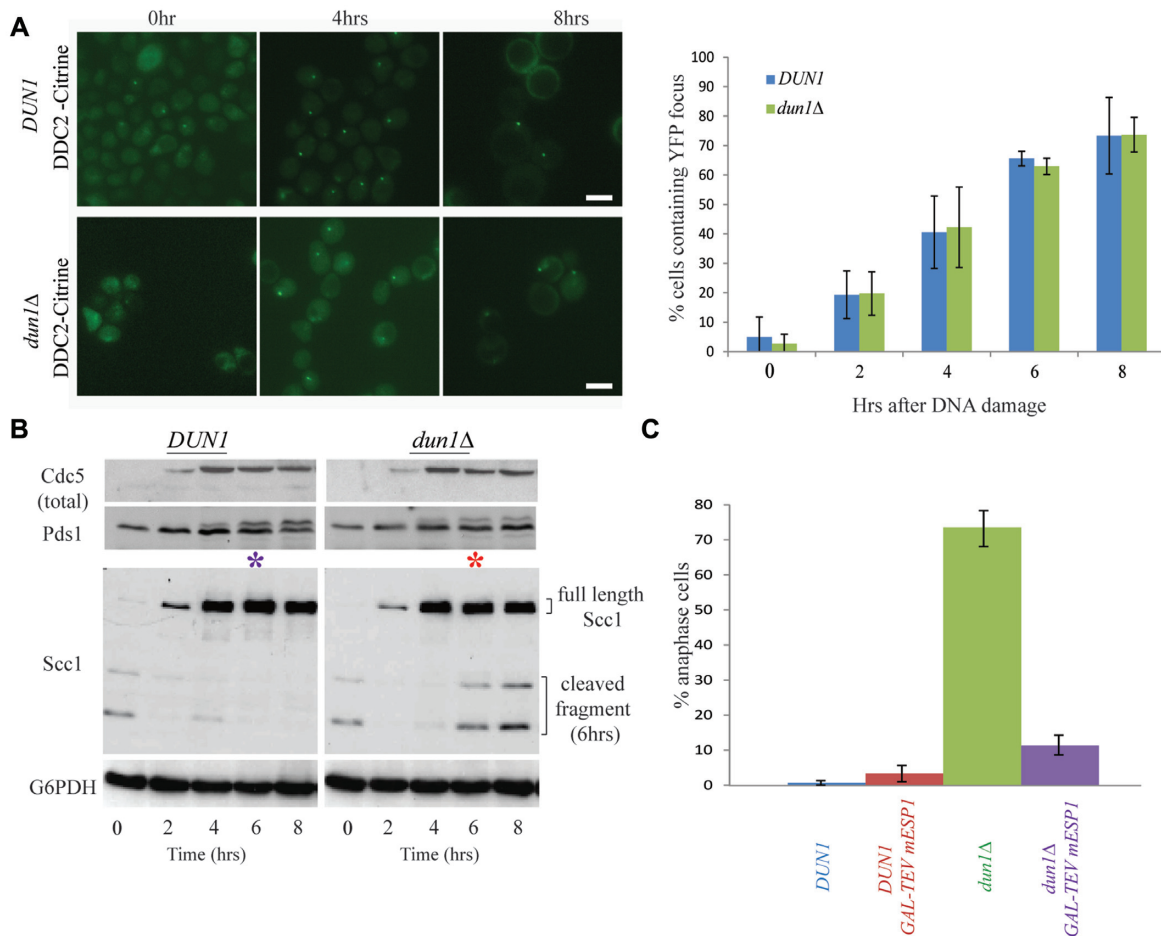
Figure 3. DNA damage signalling markers in *DUN1* deficient cells. (**A**) *DUN1* and *dun1Δ* cells harbouring endogenously tagged *DDC2-Citrine* (US6382, US6703) were synchronized in G1 by α factor treatment and released into YEP+raff+gal to induce HO-mediated DSB. Cells were harvested at regular intervals for visualization of citrine signal. Representative photomicrographs of Ddc2-Citrine during αF arrest (G1) and at 4 h and 8 h are shown (Left). The graph (right) shows the number of *DUN1* and *dun1Δ* cells containing Ddc2-citrine foci at various time intervals. Experiments were performed in triplicates ($n = 100$). The error bars correspond to standard deviation of the proportion of cells containing YFP foci (scale bar: 5 μm). (**B**) *DUN1* and *dun1Δ* strains carrying untagged *CDC5* (US5750, US6676), HA$_3$-tagged *PDS1* (US7191, US7192) or MYC$_{18}$-tagged *SCC1* (US5782, US6886) were synchronized in G1 and then released into YEP+raff+gal medium to induce HO-mediated DSB. Western blot analyses show the status of Cdc5, Pds1 and Scc1 proteins. G6PDH was used as an internal control. For the purpose of comparison, Pds1 bands in *dun1Δ* and *DUN1* cells at 6 h are marked with * and with *, respectively). For relative Pds1 densities in *DUN1* and *dun1Δ* cells, refer to Supplementary Figure S2A. (**C**) *DUN1* and *dun1Δ* cells without (US5750, US6677), or with (US8002, US8004) *mESP1* and a chromosomally integrated copy of *GAL-TEV* construct were synchronized in G1 and released at 31°C into YEP+raff+gal medium to induce the expression of HO and TEV protease. Bar graph (right) shows the percentage of cells entering anaphase 7 h after release from G1. Experiments were carried out in triplicates ($n = 100$). The error bars correspond to standard deviation of the proportion of anaphase cells at each time-point.

(Supplementary Figure S2B, upper and lower graph respectively; Supplementary Figure S2C). Collectively, these observations imply that the failure of *dun1Δ* cells to arrest in G2 upon DNA damage stems from the instability of Pds1 (and consequently Esp1-catalyzed cohesin cleavage) caused by Dun1 deficiency.

Rad53–Dun1 axis is predominantly responsible for checkpoint-mediated G2 arrest

Chk1 and Rad53 constitute the two main regulatory branches of the DNA damage checkpoint. Dun1 is placed downstream of the latter since its activation is dependent on Rad53. Previous studies have reported that Chk1 is the main kinase which phosphorylates and stabilizes Pds1 during checkpoint arrest to prevent premature chromosome

segregation (41). We sought to determine the contribution of Rad53–Dun1 axis to this regulation. Hence we analysed the dynamics of Pds1 abundance in *dun1Δ* and *chk1Δ* strains. Under normal conditions, Pds1 exists in two forms: unphosphorylated and Cdc28-phosphorylated form. In the Western blots, Pds1 appears as two bands: a lower band and a weaker higher, phosphorylated band (Supplementary Figure S3). Upon DNA damage, both bands become phosphorylated and more abundant (42). G1-synchronized *DUN1 CHK1*, *dun1Δ CHK1*, *DUN1 chk1Δ* and *dun1Δ chk1Δ* were allowed to resume cell cycle in raff+gal medium (DNA damage-condition) and the status of Pds1 and Rad53 and their ability to undergo anaphase were monitored. As anticipated, *DUN1 CHK1* cells proficiently arrested in G2, whereas >60% of *dun1Δ CHK1* cells progress to anaphase

(Figure 4A). Surprisingly, despite Chk1 deficiency *DUN1 chk1Δ* cells arrested in G2 and failed to enter mitosis. However, the addition of Dun1 deficiency, on the other hand, allowed *chk1Δ* cells (i.e. *dun1Δ chk1Δ* cells) to progress to anaphase (Supplementary Figure S4). While Rad53 is phosphorylated in all four strains to a similar extent (Figure 4A), the abundance of Pds1 exhibits stark differences. In both *DUN1 CHK1* and *DUN1 chk1Δ* cells, both Pds1 forms show marked increase in abundance at 4 h and this abundance is maintained till the end of the experiment (6 h) (Figure 4A, lower panel) (43). In *dun1Δ CHK1* cells, there is a dramatic drop in the abundance of both Pds1 forms and lower still in the *dun1Δ chk1Δ* double mutant cells (Figure 4A, lower panel). Thus, Chk1 deficiency makes no dramatic difference to the 'arrest-status' of these cells following DNA damage.

Conversely, we tested if Chk1 overexpression can compensate for Dun1 deficiency and prevent premature anaphase onset in *dun1Δ* cells. G1-synchronized *DUN1 CHK1, DUN1 chk1Δ, dun1Δ CHK1* and *dun1Δ GAL-HA$_9$-CHK1* cells were released into raff+gal medium to induce Chk1 expression (Figure 4B) and HO-mediated DSB. Rad53 was similarly phosphorylated in all strains, signifying equal activation of the checkpoint (Figure 4B). As expected, *DUN1 CHK1* and *DUN1 chk1Δ* cells arrested in G2 efficiently, while *dun1Δ CHK1* cells progressed to anaphase. Interestingly, Chk1 overexpression could not prevent mitotic onset (due to Dun1 deficiency) with *dun1Δ GAL-HA$_9$-CHK1* cells progressing to anaphase to the same extent as *dun1Δ CHK1* cells (>50% in 6 h). Taken together, these results argue that Chk1 cannot compensate for Dun1 deficiency and that Dun1 is the major contributor to Pds1 stability and execution of the checkpoint arrest, while Chk1 contributes to these responses to a limited extent.

Pds1 destabilization in *dun1Δ* cells results in diminished interactions between Pds1 and Esp1 during DNA damage
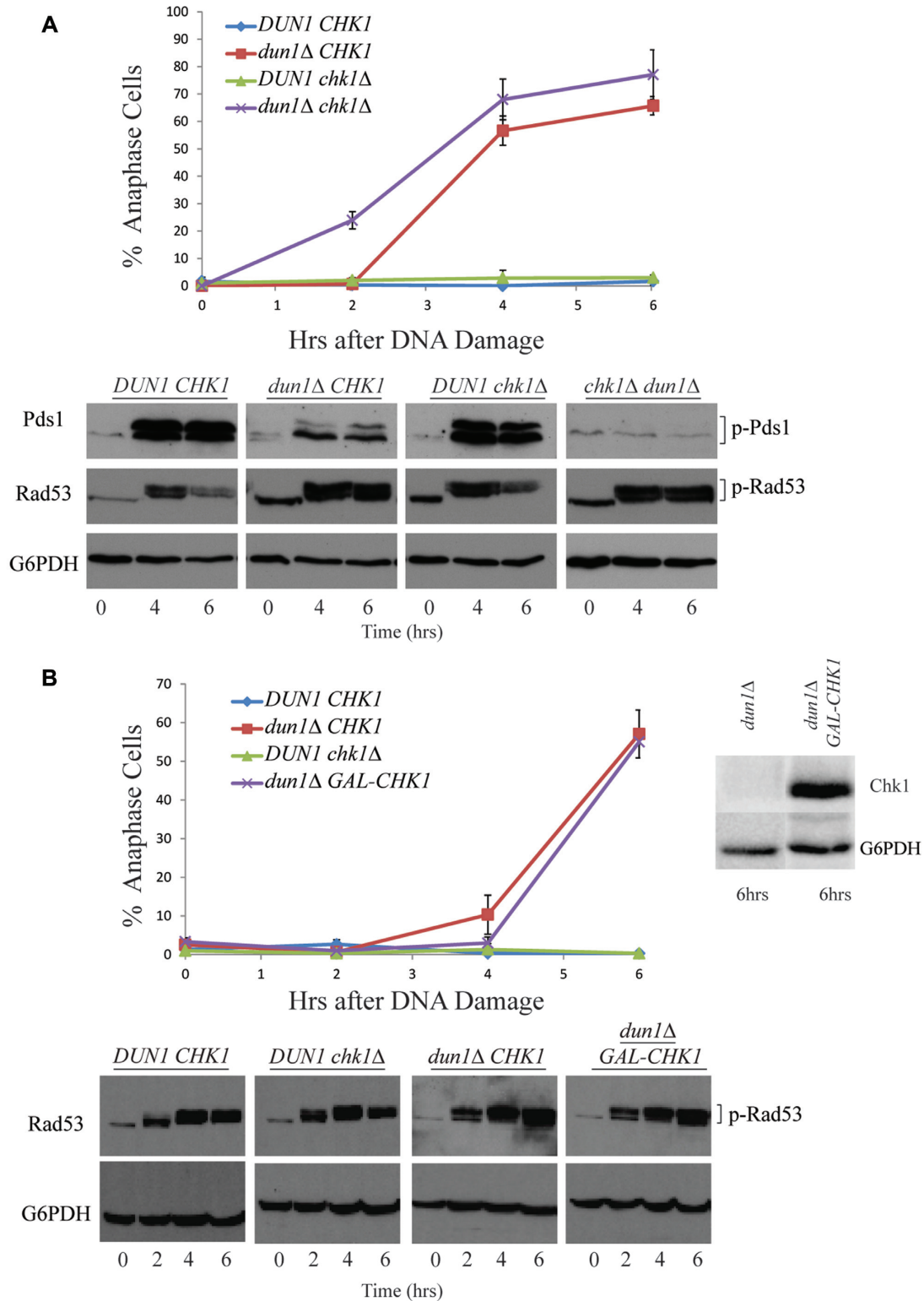
Since interaction between Pds1 and Esp1 prevents Esp1-mediated Scc1 cleavage and premature anaphase onset, we sought to confirm if lower abundance of Pds1 in *dun1Δ* cells also leads to demonstrably diminished association between Pds1 and Esp1. We tagged endogenous Pds1 and Esp1 with three copies of HA and 18 copies of MYC epitopes, respectively, in both *DUN1* and *dun1Δ* strains. To test if the behavior of the modified strains is similar to that of the unmodified versions, *DUN1 PDS1-HA$_3$ ESP1-MYC$_{18}$* and *dun1Δ PDS1-HA$_3$ ESP1-MYC$_{18}$* cells were synchronized in G1 and released into raff+gal medium to induce HO-mediated DSB. As expected, the tagged *DUN1* cells efficiently arrested in G2 and the tagged *dun1Δ* cells progressed to anaphase (Figure 5A) with somewhat enhanced cell cycle kinetics compared to that of unmodified strains (Figure 1). Consistent with this, the modified *DUN1* strain showed substantial accumulation of Pds1, while modified *dun1Δ* strain had dramatically reduced levels of Pds1 (Figure 5A, lower panel).
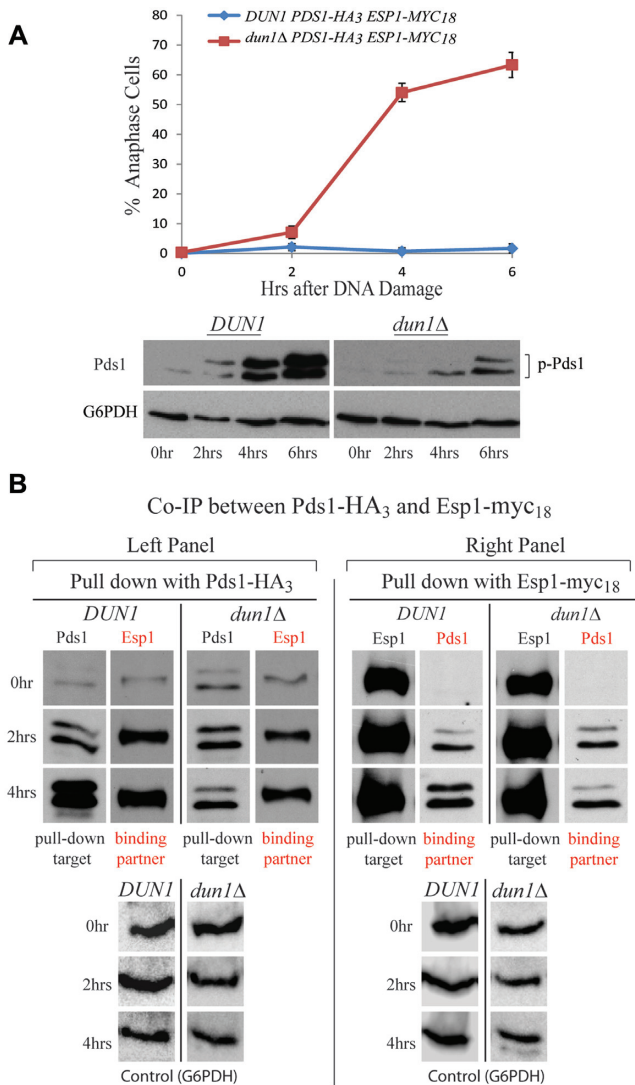
To analyse Pds1-Esp1 interaction, we performed a Co-Immunoprecipitation (Co-IP) assay. G1 synchronized *DUN1 PDS1-HA$_3$ ESP1-MYC$_{18}$* and *dun1Δ PDS1-HA$_3$ ESP1-MYC$_{18}$* cells were released in raff+gal medium (Fig-

ure 5B, Supplementary Figures S5–S7). Samples were collected at 2 h (both largely arrested in G2) and 4 h (when *dun1Δ* strain escapes G2 arrest). We first immunoprecipitated Pds1-HA$_3$ using agarose beads conjugated with anti-HA antibodies. At 2 h, similar amounts of Pds1 were detected in both *DUN1* and *dun1Δ* samples (Figure 5B, left panel; first column/second row versus third column/second row). However, more Pds1 was detected in *DUN1* cells at 4 h than in *dun1Δ* cells (Figure 5B, left panel; first column/third row versus third column/third row; relative intensity of total Pds1 levels in *DUN1* is 7.24±2.61 times with respect to total Pds1 levels in *dun1Δ* cells at 4 h). When the immunoprecipitated Pds1 was probed for its interacting partner Esp1-MYC$_{18}$, we found reduced amount of Esp1 bound to Pds1 at 4 h in *dun1Δ* cells compared to *DUN1* cells (Figure 5B, left panel; second column/third row versus fourth column/third row). Interestingly, the upper band of Pds1 in *dun1Δ* cells seems more depleted than the lower band as cells progress from 2 to 4 h time point. Quantitatively, the relative intensity of the bands (upper Pds1/total Pds1) decrease by an average of 32% (0.68±0.06-fold) in *dun1Δ* cells from 2 to 4 h (Figure 5B, left panel; third column second & third row; Supplementary Figures S6A and S7A). Reciprocally, we next immunoprecipitated Esp1-MYC$_{18}$ from *DUN1* and *dun1Δ* cell extracts using agarose beads conjugated with anti-MYC antibodies. The amount of Esp1 detected was comparable in both strains at 2 and 4 h (Figure 5B, right panel; first column/second & third row versus third column/second & third rows). The amount of Pds1 bound to Esp1, however, is significantly lower in *dun1Δ* cells at 4 h compared to *DUN1* cells (Figure 5B, right panel; 2nd column/third row versus fourth column/third row). This is consistent with the results from Pds1-HA$_3$ immunoprecipitation experiments (Figure 5B, left panel). Hence, while both *DUN1* and *dun1Δ* cells display similar amounts of Esp1, *dun1Δ* cells consistently show lower amounts of Pds1. This implies that a fraction of Esp1 is unrestrained by Pds1 in DNA damaged Dun1-deficient cells and is, therefore, free to cleave cohesin complex to induce premature chromosome segregation.

Diminished Pds1–Esp1 association in intact *dun1Δ* cells exposed to DNA damage.

Our Co-Immunoprecipitation (Co-IP) experiments show a diminished association between Esp1 and its negative regulator Pds1 in Dun1 deficient cells. To validate these findings in intact cells, we used the Bimolecular Fluorescence complementation (BiFC) assay (44). We constructed a split-Venus system where endogenous Esp1 and Pds1 were tagged with N-terminal half of Venus (Esp1-HalfVenus) and C-terminal half of Venus (HalfVenus-Pds1), respectively. Under conditions where Esp1 and Pds1 associate with each other to form a complex, the two halves of Venus interact to assemble a functional Venus tag displaying YFP signal (Figure 6A). For this experiment, four different strains were used: *DUN1 CHK1, DUN1 chk1Δ, dun1Δ CHK1* and *dun1Δ chk1Δ*. We first confirmed that the strains with endogenously tagged Esp1-HalfVenus and HalfVenus-Pds1 activate the DNA damage checkpoint as efficiently as the untagged versions, using Rad53 phosphorylation (Figures

Figure 4. Rad53-Dun1 axis is predominantly responsible for checkpoint-mediated G2 arrest. (**A**) *DUN1 CHK1* (US8094), *dun1Δ CHK1* (US8116), *DUN1 chk1Δ* (US8366) and *dun1Δ chk1Δ* (US8378) cells expressing *PDS1-HA₃* from its native promoter were synchronized in G1 and released into YEP+raff+gal medium to induce HO-mediated DSB. Bar graph shows percentage of cells entering anaphase. Experiments were performed in triplicates (*n* = 100). Lower panel: Western blot analyses of Pds1-HA₃ and Rad53, using anti-HA and anti-Rad53 antibodies respectively. (**B**) G1 synchronized *DUN1 CHK1* (US5750), *dun1Δ CHK1* (US6676), *DUN1 chk1Δ* (US8251) and *dun1Δ GAL-HA₉-CHK1* (US8267) cells were released into YEP+raff+gal medium to induce HO and Chk1 expression. Samples were harvested at regular intervals and percentage of anaphase cells was quantified. Experiments were performed in triplicates (*n* = 100). For (A) and (B), the error bars correspond to standard deviation of the proportion of anaphase cells at each time-point. Inset: Western blot analysis of galactose-induced overexpression of HA₉-Chk1 in US8267 compared to US6676. Anti-HA antibody was used to probe for HA₉-Chk1. Lower panel: Western blot analyses were performed using anti-Rad53 antibody and anti-G6PDH (loading control).

Figure 5. Pds1 destabilization and diminished interaction between Pds1 and Esp1 in the absence of *Dun1* during DNA damage. (**A**) G1 synchronized *DUN1 PDS1-HA3 ESP1-MYC18* (US8094) and *dun1Δ PDS1-HA3 ESP1-MYC18* (US8116) strains were released into YEP+raff+gal medium to induce HO-mediated DSB. Samples were harvested and number of cells in anaphase quantified. Experiments were performed in triplicates ($n = 100$), with error bars representing standard deviation of the percentage of anaphase cells at each time-point. Lower panel: Western blot analyses of Pds1-HA3 in US8094 and US8116 were performed using anti-HA antibody and anti-G6PDH (loading control). (**B**) To analyse the dynamics of Esp1–Pds1 complex, Co-Immunoprecipitation (Co-IP) assays were performed on *DUN1 PDS1-HA3 ESP1-MYC18* (US8094) and *dun1Δ PDS1-HA3 ESP1-MYC18* (US8116) cells. Cells from the experiment described in (A) were harvested, processed and incubated with either anti-MYC or anti-HA antibody-conjugated agarose beads. The immune-complexes were analysed by gel electrophoresis for the levels of Esp1-MYC18 and Pds1-HA3 proteins. Lower panel: As a loading control, 20 µl of each cell lysate used for immunoprecipitation (0.5 mg/reaction) were analysed for G6PDH levels.

6B, 4A). Fluorescence microscopy revealed that, with the exception of *dun1Δ chk1Δ* cells, the fraction of cells with YFP signal increased in all strains in the 2–4 h window (Figure 6C, D). While the proportion of cells with YFP signal continued to increase in both *DUN1 CHK1* (100%) and

DUN1 chk1Δ (80%) cells, the signal in *dun1Δ CHK1* began to decline after 4 h and reached ∼50% of its peak value at 7 h (Figure 6C). The signal in *dun1Δ chk1Δ* double mutant cells was barely visible and this remained so throughout the course of the experiment (Figure 6C, D). We noticed that the intensity of the YFP signal in *dun1Δ CHK1* was consistently lower than in *DUN1 CHK1* and *DUN1 chk1Δ* cells suggesting that, in the absence of Dun1, Esp1–Pds1 association is lower or relatively unstable. Together, the Co-IP and BiFC experiments imply that the Pds1–Esp1 association in the DNA-damaged *dun1Δ* cells is 'less in its extent' or weaker so that Esp1 is relatively free from Pds1-mediated inhibition to induce premature chromosome segregation. It is noteworthy that while Chk1 deficiency alone does not influence the Pds1 abundance or Pds1–Esp1 association significantly, its effect on these parameters is additive when combined with a deficiency in the main 'influencer' Dun1.

Inactivation of E3 ligase Rsp5 restores checkpoint arrest and Pds1 abundance in DNA-damaged *dun1Δ* cells

One interpretation of our results is that the premature onset of anaphase in *dun1Δ* cells stems from the low abundance of Pds1 caused by its heightened proteolytic degradation. During normal mitosis, the E3 ligase anaphase-promoting complex (APC), together with its co-activator Cdc20, is responsible for poly-ubiquitylation of many mitotic substrates leading to their proteolysis, including Pds1 (45). We tested if APC^{Cdc20} is responsible for the low levels of Pds1 in DNA-damaged *dun1Δ* cells. This can be tested by introducing a temperature-sensitive allele of APC subunit Cdc23 (i.e. *cdc23-1*) in *dun1Δ* strain. Unfortunately, all our attempts to introduce *cdc23-1* mutation in the strains with JKM139 genetic background (using HO to induce DNA damage) were unsuccessful, prompting us to adopt a different experimental strategy for DNA damage and checkpoint activation. G1-synchronized *DUN1 CDC23* cells were released into YEPD medium containing spindle poison Nocodazole. Once arrested in mitosis with a single nucleus, 2N DNA content and no mitotic spindle, cells were treated with DNA damaging agent MMS (methyl methanesulfonate) for 30 min, then washed and released into fresh YEPD medium with or without MMS in the absence of Nocodazole. Cells released in the presence of MMS activated the DNA damage checkpoint (as indicated by Rad53 phosphorylation) and remained arrested in metaphase whereas those released in the absence of MMS eventually entered anaphase (Figure 7A). This suggests that when subjected to DNA damage, mitotically arrested cells can efficiently activate DNA damage checkpoint and prevent anaphase onset.

We employed this experimental regime to ask if Pds1 degradation in DNA damaged *dun1Δ* cells is APC dependent. G1 synchronized *DUN1 CDC23*, *dun1Δ CDC23*, *DUN1 cdc23-1* and *dun1Δ cdc23-1* cells were released into Nocodazole containing YEPD medium and then treated with MMS. Subsequently, cells were washed and released into MMS containing medium at 37°C to inactivate mutant Cdc23. As anticipated, *DUN1 CDC23* and *DUN1 cdc23-1* remained arrested in metaphase, whereas *dun1Δ CDC23* cells progressed to anaphase. Surprisingly, *dun1Δ cdc23-1* cells also entered anaphase, albeit at a rate somewhat slower
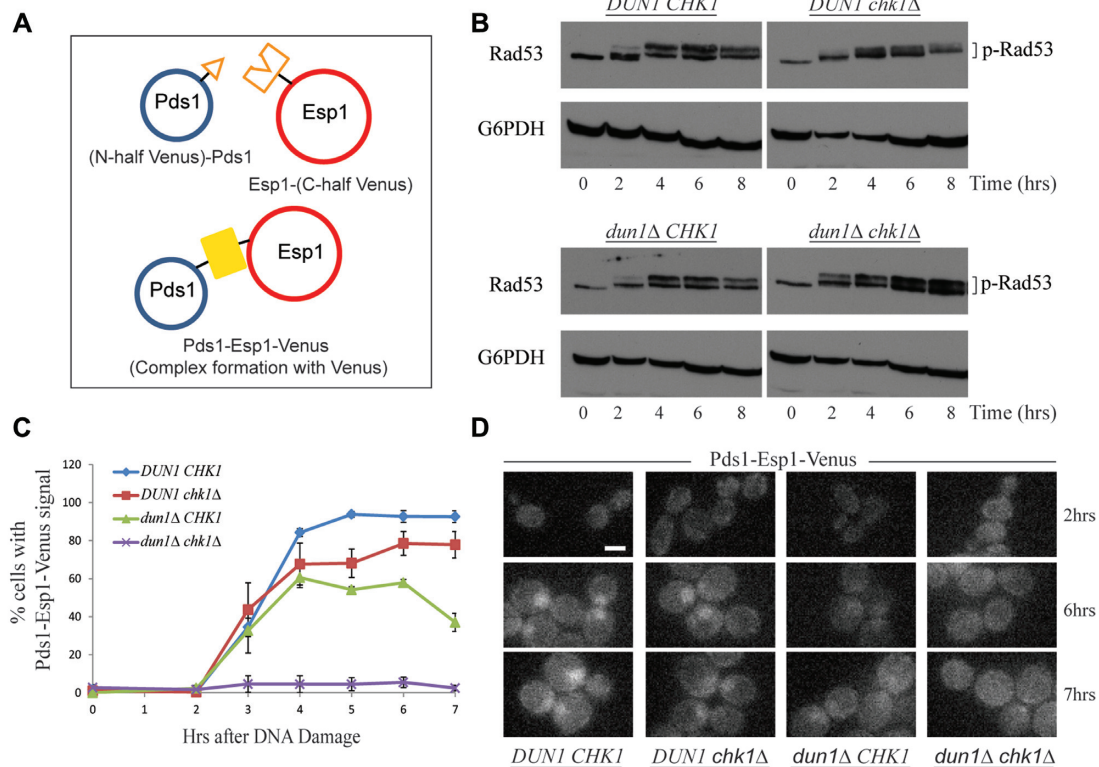
Figure 6. Diminished Pds1–Esp1 association in *dun1Δ* cells exposed to DNA damage. (**A**) A schematic diagram depicting the use of BiFC to observe Esp1 and Pds1 interaction *in vivo*. Pds1 was N-terminally tagged with the first-half of Venus tag, (N'-half Venus-Pds1), while Esp1 was tagged at the C-terminus with the second-half of Venus tag (Esp1-C'half Venus). When Esp1:Pds1 complexes are formed, the two halves of the Venus will combine to form a functional Venus, resulting in a YFP signal. (**B**) *DUN1 CHK1* (US8318), *DUN1 chk1Δ* (US8422), *dun1Δ CHK1* (US8334), *dun1Δ chk1Δ* (US8457) strains containing both Venus-tagged *PDS1* and *ESP1* (as described above) were synchronized in G1 and then released into YEP+raff+gal medium to induce HO expression. Samples at 2 h intervals were harvested and used for Western blots analyses, using anti-Rad53 antibody. (**C**) Samples collected from the experiment described in (**B**) were imaged immediately after collection. Graph shows percentage of cells containing the YFP signal (signifying Esp1:Pds1 complex formation). Experiments were performed in triplicates ($n = 100$), with error bars corresponding to standard deviation of the proportion of cells with a positive YFP signal at each time-point. (**D**) Representative photomicrographs showing YFP signal at 2 h, 6 h and 7 h in cells from strains described above (scale bar: 5 μm).

than *dun1Δ CDC23* cells. This implies that anaphase onset in Dun1 deficient cells occurs independently of APC activity (Figure 7B, upper panel). We asked that if APC does not catalyse anaphase entry in DNA-damaged *dun1Δ* cells, what other E3 ligase is responsible for anaphase onset. A previous 'high throughput' study had reported an interaction between Dun1 and HECT domain containing E3 ligase Rsp5 (26); however, the significance of this interaction is not known. Essential for viability, Rsp5 is a yeast homolog of human Nedd4 and is implicated in a number of cellular processes including the UV-induced RNA polymerase II ubiquitylation and degradation (26,46). To determine if Rsp5 is involved in anaphase onset in Dun1 deficient cells, we used a temperature sensitive allele *rsp5-1*, which carries a point mutation in the HECT catalytic domain. We subjected *DUN1 RSP5*, *dun1Δ RSP5*, *DUN1 rsp5-1 and dun1Δ rsp5-1* strains to the experimental regime outlined above and monitored the cells for their ability to progress to anaphase. Following MMS treatment, cells were released at 37°C to inactivate Rsp5-1 protein. As expected, while *DUN1 RSP5* and *DUN1 rsp5-1* cells remained arrested at metaphase, *dun1Δ RSP5* cells efficiently transited to anaphase. Interestingly, *dun1Δ rsp5-1* remained ar-

rested in metaphase suggesting that inactivation of Rsp5 prevents *dun1Δ* cells from undergoing anaphase and restores the metaphase arrest (Figure 7B, lower panel; Supplementary Figure S8). To test if Rsp5 inactivation also restores G2 arrest in *dun1Δ* cells incurring a HO-induced DSB (in JKM179 background), G1-synchronized cells were released at 24°C into raff+gal medium for 2 h to induce HO expression, before shifting them to 37°C to inactivate Rsp5. As anticipated, *DUN1 RSP5* and *DUN1 rsp5-1* cells arrested at G2 and *dun1Δ RSP5* cells promptly transited to anaphase. Once again, consistent with the results described above (Figure 7B), *dun1Δ rsp5-1* arrested in G2, implying that inactivation of Rsp5 reinstates the checkpoint-induced G2 arrest in *dun1Δ* (Figure 7C, graph). The inactivation of Rsp5 in *dun1Δ* cells also stabilizes Pds1 and restores its abundance (Figure 7C, middle panel). To ensure that Pds1 stability is indeed Rsp5 dependent, one-half of the *DUN1 RSP5*, *DUN1 rsp5-1* and *dun1Δ rsp5-1* cultures that had arrested in G2 at 37°C with stabilized Pds1, were shifted to 24°C to restore Rsp5 function. After the shift to 24°C, *DUN1 RSP5 and DUN1 rsp5-1* cells remain arrested and Western blots revealed an increase in intensities of the Pds1 bands (Figure 7C, lower panel, left and middle sections).
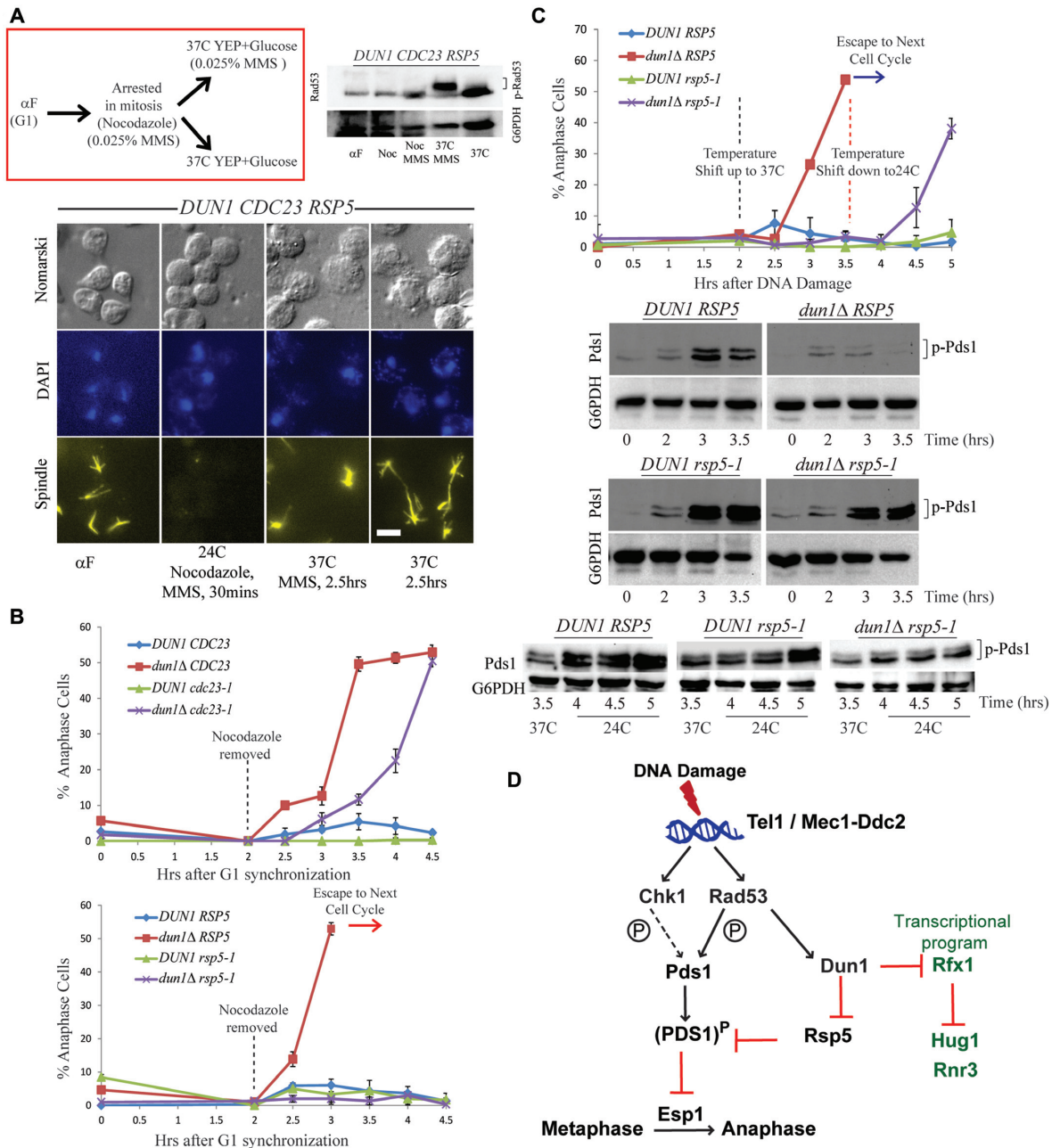
Figure 7. Inactivation of E3 ligase Rsp5 restores checkpoint arrest and Pds1 abundance in Dun1 deficient cells. (**A**) Experimental protocol to investigate DNA damage checkpoint in cells synchronized in mitosis. G1 synchronized cells were released into YEP+raff medium containing Nocodazole for 2 h to allow for mitotic arrest (single nucleus and no mitotic spindle) at 25°C. Methyl Methanesulfonate (MMS; 0.025%) was added for 0.5 h to induce DNA damage after which Nocodazole was removed and cells were released into fresh medium at 37°C with or without 0.025% MMS. Top right panel: Western blot analysis of *DUN1* (US5880) cells containing Rad53-HA₂, probed using anti-HA antibody showed phosphorylated Rad53 (activated) in presence of MMS and dephosphorylated (not activated) in absence of MMS. Lower: representative photomicrographs of the cells at various stages (scale bar: 5 μm). (**B**) Upper graph: *DUN1 CDC23* (US8094), *dun1Δ CDC23* (US8116), *DUN1 cdc23-1* (US1573), and *dun1Δ cdc23-1* (US9085) cells were treated as described in (A). After 2 h of Nocodazole treatment at 24°C, Nocodazole was removed and cells were incubated at 37°C in 0.025% MMS to inactivate *cdc23-1* mutation. Graph shows percentage of cells in anaphase at 30 min intervals after Nocodazole incubation. Experiments were performed in triplicates (*n* = 100). Lower graph: *DUN1 RSP5* (US1363), *dun1Δ RSP5* (US4909), *DUN1 rsp5-1* (US9101) and *dun1Δ rsp5-1* (US9372) were treated and analyzed similarly. (**C**) Endogenous *RSP5* was replaced by the temperature sensitive *rsp5-1* allele in *DUN1* and *dun1Δ* strains with JKM179 genetic background. *DUN1 RSP5* PDS1-HA₃ (US9269), *dun1Δ RSP5 PDS1-HA₃* (US9271), *DUN1 rsp5-1 PDS1-HA₃* (US9279) and *dun1Δ rsp5-1 PDS1-HA* (US9292) cells were synchronized in G1 (0 h) at 24°C, followed by release into YEP+raff+gal medium for 2 h, before shifting to 37°C to inactivate the mutant Rsp5 protein. After 1.5 h at 37°C (3.5 h timepoint), half of the culture was shifted back to 24°C to re-activate the mutant Rsp1 for another 1.5 h (5 h timepoint). Graph shows percentage of cells entering anaphase in samples harvested at 30 min intervals. Using anti-HA antibody, Western blot analyses were performed to observe the state of phospho-Pds1. Top and middle Western blots show dynamics of Pds1 during G1 arrest and after release into 37°C. Lower panel: Western blot analysis shows dynamics of Pds1 after the cells were shifted to 24°C to reactivate the mutant Rsp5. These experiments were performed in triplicates (n = 100). For both (B) and (C), the error bars correspond to standard deviation of the proportion of anaphase cells at each time-point. (**D**) A proposed regulatory scheme. Please see text for details.

The *dun1Δ rsp5-1* cells that were retained at 37°C until the 5 h time-point also remained arrested (data not shown). However, ∼40% of *dun1Δ rsp5-1* cells (5 h time-point in Figure 7C, graph), progressed to anaphase 1.5 h after the shift to 24°C and correspondingly, Pds1 levels were signigicantly lower than those in *DUN1 RSP5 and DUN1 rsp5-1* cells (Figure 7C, lower panel, rightmost section). Together, these observations raise a strong possibility that (i) anaphase onset in DNA-damaged *dun1Δ* cells is predominantly due to Pds1 destabilization and (ii) Rsp5, not APC, catalyses the destabilization of Pds1 in *dun1Δ*.

DISCUSSION

Halting cell cycle progression at G2 in response to DNA damage suffered during S phase is an integral part of the checkpoint control. In yeast, the currently accepted model designates checkpoint kinases Chk1 and Rad53 as critical regulators that prevent premature segregation of damaged chromosomes until they are appropriately repaired. However, our results show that Dun1 deficient cells successfully detect the damage signal (Figure 3) and activate the transducer kinases Chk1 and Rad53 (Figure 1), but yet fail to arrest in G2 and proceed to anaphase with damaged chromosomes. This implies a critical involvement of Dun1 in the imposition of G2 arrest.

Phosphorylation of Pds1, rendering it resistant to APC-mediated proteolysis, is one of the central events in the inhibition of premature onset of anaphase. According to the previous reports, Pds1 is phosphorylated primarily by Chk1 during DNA damage (20). In our experimental regime, while *dun1Δ* cells escape from checkpoint arrest between 4 and 6 h (Figures 4 and 5), cells lacking Chk1 remain arrested in pre-anaphase state (Figure 4). Moreover, *chk1Δ* cells show only a marginal decrease in Pds1 phosphorylation (Figure 4A). This is consistent with the observations that (i) overexpression of Chk1 fails to restore G2 arrest in *dun1Δ* cells (Figure 4) and (ii) Chk1 deficiency has only a muted effect on Pds1/Esp1 association in the BiFC assay (Figure 6). However, the abundance of phosphorylated Pds1 is dramatically reduced in *dun1Δ* cells. This is also reflected in the reduced association of Pds1–Esp1 in the Dun1 deficient cells (Figure 5, 6), indicating that Dun1′s role in the execution of G2 arrest is linked to the maintenance of phosphorylated Pds1 stability and not to its function in DNA damaged-induced transcription (Figure 2). Collectively our results suggest that Dun1 is a key determinant of Pds1 stability and cell cycle arrest where Chk1 makes a limited contribution (Figure 7D).

If Chk1 has a limited role in Pds1 phopshorylation and cell cycle arrest, it can be argued that Rad53–Dun1 axis is mainly responsible for the DNA-damage induced phosphorylation of Pds1. However, under the conditions where Pds1 degradation is inhibited (Figure 7C), phosphorylated Pds1 is present in substantial amounts in *dun1Δ* cells, indicating that Dun1 may not be the main kinase responsible for Pds1 phosphorylation during DNA damage. This function is perhaps most likely served by checkpoint-activated Rad53 (Figure 7D). Previous studies have also reported some involvement of Cdc28 kinase in Pds1 phosphorylation (29), significance of which is unclear at present. It is noteworthy that although Rad53 is substantially phosphorylated and activated in *dun1Δ* cells, lower amounts of phosphorylated Rad53 are observed particularly after their escape from cell cycle arrest from 6 h onward (Figures 1C, 2A). This is likely due to the actions of mitotic phosphatases which act to reverse activated kinases after chromosome segregation (47).

Our conclusion that Dun1–Rad53 axis plays a key regulatory role in imposing G2 arrest during DNA damage is consistent with previous reports (48) which suggested that Rad53 and Dun1 act in the same pathway that imposes DNA-damage induced cell cycle arrest. These studies also suggested that Rad53-Dun1 and Pds1 constitute two parallel pathways (43,49). However, Dun1′s exact role in the execution of the cell cycle arrest was unclear. Our results clearly show that Pds1 is highly unstable in DNA-damaged *dun1Δ* cells. That a substantial decline in Pds1 levels in *dun1Δ* cells involves both phosphorylated bands (Figures 4 and 5), imply that Pds1 may not undergo dephosphorylation prior to proteolytic degradation. However, phosphorylated Pds1 is known to be resistant to APC-mediated proteolysis. This together with our observation that inactivation of APC does not prevent anaphase escape in damaged *dun1Δ* cells (Figure 7B, upper graph) suggest that degradation of phospho-Pds1 is not APC dependent. These results raise an important issue: how is APC-resistant phosphorylated Pds1 degraded, releasing Esp1 and catalysing chromosome segregation in Dun1 deficient cells? A previous study, involving a high throughput mass-spectrometry, had reported a physical interaction between Dun1 and the Nedd4 family E3 ligase Rsp5 (25,26). We find that inactivation of Rsp5 in *dun1Δ* cells not only prevents premature anaphase onset but also restores the abundance of phosphorylated Pds1 (Figure 7). This strongly suggest that Rsp5 is the E3 ubiquitin ligase which mediates the proteolytic degradation of APC-resistant phosphorylated Pds1 during cells' escape from DNA-damage induced G2 arrest. Rsp5, an essential gene, is involved in a number of cellular functions, including heat shock response, endocytosis, ribosomal stability and turnover of RNA Pol II subunit Rbp1 during DNA damage (24,46). It is interesting that yeast cells use for a specific task in DDR a protein involved in multiple cellular processes.

Nevertheless, these results, together with previously reported findings, are consistent with a simple regulatory scheme (Figure 7D) in which checkpoint activated Rad53 is the predominant kinase mediating Pds1 phosphorylation, with Chk1 playing a limited role. Phosphorylated Pds1 associates with the separase Esp1 and prevent it from cleaving cohesin subunit Scc1, precluding transition to anaphase. Rad53 also activates Dun1 (as shown by previous studies) which in turn accomplishes two important tasks: (i) inhibition of transcription repressor Rfx1 to induce transcription of genes such as *HUG1* and *RNR3* (ii) inactivation of HECT domain containing E3 ligase Rsp5 to stabilize Pds1/Esp1 complex (24,50). Whether Dun1 inactivates Rsp5 by direct phosphorylation or if Rsp5 directly mono- or poly-ubiquitylates phosphorylated Pds1 are subjects of further investigations. We note that though this regulatory framework accounts for the behaviour of Dun1 deficient cells in various experimental conditions used in this

study, anaphase progression in *dun1Δ* cells is somewhat different from cells undergoing anaphase after DNA repair. While *dun1Δ* cells proceed to anaphase in the presence of activated checkpoint (Figure 1), cells that have completed DNA repair do so after extinguishing the checkpoint. It is possible that the regulatory nuances of anaphase initiation in the two contexts differ to some extent. Since there is no firm evidence thus far for the existence of a phosphorylated Pds1-specific phosphatase that would reinstate 'APC-mediated onset of anaphase' in post-repair cells, we believe that E3 ligase Rsp5 may be a critical element in cells' attempt to overcome G2 arrest in both pre- and post-repair conditions.

It is curious that *S. cerevisiae* requires both Rad53 and its paralog Dun1 to execute the cell cycle arrest in response to chromosome damage. Since Dun1 lacks the SQ/TQ cluster domains (SCD1 and SCD2) that are present in Rad53, it is possible that *DUN1* emerged from *RAD53* duplication, followed by the loss of SCD1 and SCD2 domains and functional diversification. However, paralog pairs can also originate from whole genome duplication (51,52), followed by functional divergence of the duplicates. *S. cerevisiae* genome is reported to have resulted from whole genome duplication of a common ancestor it shares with the yeast *Ashbya gossypii* (53). *A. gossypii* genome, which has not undergone whole genome duplication, contains *DUN1* (on chromosome VI, AFL188C). This implies that Dun1 serves some fundamental function(s) to have been conserved through the 'distant but evolutionarily related' lineages that split ∼100 mya ago and gave rise to *S. cerevisiae*, *A gossypii* and *K. lactis*. Given that *DUN1* is non-essential for vegetative growth, its functions may be necessary for specific physiological context such as DDR. While Dun1′s function in DNA damage-induced transcription is well established, this study has uncovered another function of Dun1 in the stabilization of Pds1/Esp1 complex, essential for an effective G2/M arrest in response to chromosomal damage. In addition, the E3 ligase Rsp5 emerges as an important regulator in the DNA damage response.

DATA AVAILABILITY

WinMBI is an open source software produced by Purdue University and is available at https://winmdi.software.informer.com/2.8/. Imagej is a open source Java-based image processing program codeveloped by the National Institutes of Health and the Laboratory for Optical and Computational Instrumentation. Imagej can be assessed at https://imagej.nih.gov/ij/index.html.

SUPPLEMENTARY DATA

Supplementary Data are available at NAR Online.

ACKNOWLEDGEMENTS

FUNDING

REFERENCES

1. Jackson,S.P. and Bartek,J. (2009) The DNA-damage response in human biology and disease. *Nature*, **461**, 1071–1078.
2. Basu,A.K. (2018) DNA damage, mutagenesis and cancer. *Int. J. Mol. Sci.*, **19**, 970.
3. Hoeijmakers,J.H.J. (2001) Genome maintenance mechanisms for preventing cancer. *Nature*, **411**, 366–374.
4. Ciccia,A. and Elledge,S.J. (2010) The DNA damage response: making it safe to play with knives. *Mol. Cell*, **40**, 179–204.
5. Zhou,C., Elia,A.E., Naylor,M.L., Dephoure,N., Ballif,B.A., Goel,G., Xu,Q., Ng,A., Chou,D.M., Xavier,R.J. *et al.* (2016) Profiling DNA damage-induced phosphorylation in budding yeast reveals diverse signaling networks. *Proc. Natl. Acad. Sci. U.S.A.*, **113**, E3667–E3675.
6. McKinnon,P.J. (2012) ATM and the molecular pathogenesis of ataxia telangiectasia. *Annu. Rev. Pathol.*, **7**, 303–321.
7. Stracker,T.H., Roig,I., Knobel,P.A. and Marjanovic,M. (2013) The ATM signaling network in development and disease. *Front. Genet.*, **4**, 37.
8. Majka,J. and Burgers,P. (2003) Yeast rad17/Mec3/Ddc1: a sliding clamp for the DNA damage checkpoint. *Proc. Natl. Acad. Sci. U.S.A.*, **100**, 2249–2254.
9. Majka,J., Niedziela-Majka,A. and Burgers,P.M. (2006) The checkpoint clamp activates Mec1 kinase during initiation of the DNA damage checkpoint. *Mol. Cell*, **24**, 891–901.
10. Paciotti,V., Clerici,M., Lucchini,G. and Longhese,M. (2000) The checkpoint protein Ddc2, functionally related to S. pombe Rad26, interacts with Mec1 and is regulated by Mec1-dependent phosphorylation in budding yeast. *Genes Dev.*, **14**, 2046–2059
11. Blankley,R.T. and Lydall,D. (2004) A domain of Rad9 specifically required for activation of Chk1 in budding yeast. *J. Cell Sci.*, **117**, 601–608.
12. Squire,C.J., Dickson,J.M., Ivanovic,I. and Baker,E.N. (2005) Structure and inhibition of the human cell cycle checkpoint kinase, Wee1A kinase: an atypical tyrosine kinase with a key role in CDK1 regulation. *Structure*, **13**, 541–550.
13. Peng,C., Graves,P.R., Thoma,R.S., Wu,Z., Shaw,A.S. and Piwnica-Worms,H. (1997) Mitotic and G2 checkpoint control: regulation of 14-3-3 protein binding by phosphorylation of Cdc25C on serine-216. *Science*, **277**, 1501–1505.
14. Zhou,B. and Elledge,S. (2000) The DNA damage response: putting checkpoints in perspective. *Nature*, **408**, 433–439.
15. Finn,K., Lowndes,N.F. and Grenon,M. (2012) Eukaryotic DNA damage checkpoint activation in response to double-strand breaks. *Cell Mol. Life Sci.*, **69**, 1447–1473.
16. Tang,X. and Wang,Y. (2006) Pds1/Esp1-dependent and -independent sister chromatid separation in mutants defective for protein phosphatase 2A. *Proc. Natl. Acad. Sci. U.S.A.*, **103**, 16290–16295.
17. Zhou,Z. and Elledge,S. (1993) DUN1 encodes a protein kinase that controls the DNA damage response in yeast. *Cell*, **75**, 1119–1127.
18. Shirayama,M., Tóth,A., Gálová,M. and Nasmyth,K. (1999) APC(Cdc20) promotes exit from mitosis by destroying the anaphase inhibitor Pds1 and cyclin Clb5. *Nature*, **402**, 203–207.
19. Uhlmann,F., Wernic,D., Poupart,M., Koonin,E. and Nasmyth,K. (2000) Cleavage of cohesin by the CD clan protease separin triggers anaphase in yeast. *Cell*, **103**, 375–386.
20. Wang,H., Liu,D., Wang,Y., Qin,J. and Elledge,S.J. (2001) Pds1 phosphorylation in response to DNA damage is essential for its DNA damage checkpoint function. *Genes Dev.*, **15**, 1361–1372.

21. Andreson,B.L., Gupta,A., Georgieva,B.P. and Rothstein,R. (2010) The ribonucleotide reductase inhibitor, Sml1, is sequentially phosphorylated, ubiquitylated and degraded in response to DNA damage. *Nucleic Acids Res.*, **38**, 6490–6501.

22. Zhao,X. and Rothstein,R. (2002) The Dun1 checkpoint kinase phosphorylates and regulates the ribonucleotide reductase inhibitor Sml1. *Proc. Natl. Acad. Sci. U.S.A.*, **99**, 3746–3751.

23. Basrai,M., Velculescu,V., Kinzler,K. and Hieter,P. (1999) NORF5/HUG1 is a component of the MEC1-mediated checkpoint response to DNA damage and replication arrest in Saccharomyces cerevisiae. *Mol. Cell Biol.*, **19**, 7041–7049.

24. Lee,H., Yuan,C., Hammet,A., Mahajan,A., Chen,E., Wu,M., Su,M., Heierhorst,J. and Tsai,M. (2008) Diphosphothreonine-specific interaction between an SQ/TQ cluster and an FHA domain in the Rad53-Dun1 kinase cascade. *Mol. Cell*, **30**, 767–778.

25. Beaudenon,S., Huacani,M., Wang,G., McDonnell,D. and Huibregtse,J. (1999) Rsp5 ubiquitin-protein ligase mediates DNA damage-induced degradation of the large subunit of RNA polymerase II in Saccharomyces cerevisiae. *Mol. Cell Biol.*, **19**, 6972–6979.

26. Yuen,H., Albrecht,G., Adrian,H., Gary,D.B., Lynda,M., Sally-Lin,A., Anna,M., Paul,T., Keiryn,B., Kelly,B. *et al.* (2002) Systematic identification of protein complexes in Saccharomyces cerevisiae by mass spectrometry. *Nature*, **415**, 180–183.

27. Agarwal,R., Tang,Z., Yu,H. and Cohen-Fix,O. (2003) Two distinct pathways for inhibiting pds1 ubiquitination in response to DNA damage. *J Biol. Chem.*, **278**, 45027–45033.

28. Lee,S., Moore,J., Holmes,A., Umezu,K., Kolodner,R. and Haber,J. (1998) Saccharomyces Ku70, mre11/rad50 and RPA proteins regulate adaptation to G2/M arrest after DNA damage. *Cell*, **894**, 399–409.

29. Moore,J. and Haber,J. (1996) Cell cycle and genetic requirements of two pathways of nonhomologous end-joining repair of double-strand breaks in Saccharomyces cerevisiae. *Mol. Cell Biol.*, **16**, 2164–2173.

30. Griesbeck,O., Baird,G.S., Campbell,R.E., Zacharias,D.A. and Tsien,R.Y. (2001) Reducing the environmental sensitivity of yellow fluorescent protein. Mechanism and applications. *J. Biol. Chem.*, **276**, 29188–29194.

31. Rekas,A., Alattia,J.R., Nagai,T., Miyawaki,A. and Ikura,M. (2002) Crystal structure of venus, a yellow fluorescent protein with improved maturation and reduced environmental sensitivity. *J. Biol. Chem.*, **277**, 50573–50578.

32. Zaim,J., Speina,E. and Kierzek,A.M. (2005) Identification of new genes regulated by the Crt1 transcription factor, an effector of the DNA damage checkpoint pathway in Saccharomyces cerevisiae. *J. Biol. Chem.*, **280**, 28–37.

33. Zhang,Z. and Reese,J.C. (2005) Molecular genetic analysis of the yeast repressor Rfx1/Crt1 reveals a novel two-step regulatory mechanism. *Mol. Cell Biol.*, **25**, 7399–7411.

34. Woolstencroft,R.N., Beilharz,T.H., Cook,M.A., Preiss,T., Durocher,D. and Tyers,M. (2006) Ccr4 contributes to tolerance of replication stress through control of CRT1 mRNA poly(A) tail length. *J. Cell Sci.*, **119**, 5178–5192

35. Deshpande,I., Seeber,A., Shimada,K., Keusch,J.J., Gut,H. and Gasser,S.M. (2017) Structural basis of Mec1-Ddc2-RPA assembly and activation on Single-Stranded DNA at sites of damage. *Mol. Cell*, **68**, 431–445.

36. Donnianni,R., Ferrari,M., Lazzaro,F., Clerici,M., Tamilselvan,N.B., Plevani,P., Muzi-Falconi,M. and Pellicioli,A. (2010) Elevated levels of the polo kinase Cdc5 override the Mec1/ATR checkpoint in budding yeast by acting at different steps of the signaling pathway. *PLoS Genet.*, **6**, e1000763.

37. Zhang,T., Nirantar,S., Lim,H.H., Sinha,I. and Surana,U. (2009) DNA damage checkpoint maintains CDH1 in an active state to inhibit anaphase progression. *Dev. Cell*, **17**, 541–551.

38. Sun,Y., Kucej,M., Fan,H.Y., Yu,H., Sun,Q.Y. and Zou,H. (2009) Separase is recruited to mitotic chromosomes to dissolve sister chromatid cohesion in a DNA-dependent manner. *Cell*, **137**, 123–132.

39. Kostallas,G., Löfdahl,P.-Å. and Samuelson,P. (2011) Substrate profiling of tobacco etch virus protease using a novel fluorescence-assisted whole-cell assay. *PLoS One.*, **6**, e16136.

40. Makrantoni,V. and Marston,A.L. (2018) Cohesin and chromosome segregation. *Curr. Biol.*, **28**, R688–R693.

41. Sanchez,Y., Bachant,J., Wang,H., Hu,F., Liu,D., Tetzlaff,M. and Elledge,S. (1999) Control of the DNA damage checkpoint by chk1 and rad53 protein kinases through distinct mechanisms. *Science*, **286**, 1166–1171.

42. Agarwal,R. and Cohen-Fix,O. (2002) Phosphorylation of the mitotic regulator Pds1/securin by Cdc28 is required for efficient nuclear localization of Esp1/separase. *Genes Dev.*, **16**, 1371–1382.

43. Cohen-Fix,O. and Koshland,D. (1997) The anaphase inhibitor of Saccharomyces cerevisiae Pds1p is a target of the DNA damage checkpoint pathway. *Proc. Natl. Acad. Sci. U.S.A.*, **94**, 14361–14366.

44. Sung,M.K. and Huh,W.K. (2007) Bimolecular fluorescence complementation analysis system for in vivo detection of protein-protein interaction in Saccharomyces cerevisiae. *Yeast*, **24**, 767–775.

45. Prinz,S., Hwang,E., Visintin,R. and Amon,A. (1998) The regulation of Cdc20 proteolysis reveals a role for APC components Cdc23 and Cdc27 during S phase and early mitosis. *Curr. Biol.*, **8**, 750–760.

46. Wang,G., Yang,J. and Huibregtse,J. (1999) Functional domains of the Rsp5 ubiquitin-protein ligase. *Mol Cell Biol.*, **19**, 342–352.

47. Travesa,A., Duch,A. and Quintana,D.G. (2008) Distinct phosphatases mediate the deactivation of the DNA damage checkpoint kinase Rad53. *J. Biol. Chem.*, **283**, 17123–17130.

48. Jia,X., Weinert,T. and Lydall,D. (2004) Mec1 and Rad53 inhibit formation of single-stranded DNA at telomeres of Saccharomyces cerevisiae cdc13-1 mutants. *Genetics*, **166**, 753–764.

49. Gardner,R., Putnam,C.W. and Weinert,T. (1999) RAD53, DUN1 and PDS1 define two parallel G2/M checkpoint pathways in budding yeast. *EMBO J.*, **18**, 3173–3185.

50. Chen,S.H., Smolka,M.B. and Zhou,H. (2007) Mechanism of Dun1 activation by Rad53 phosphorylation in Saccharomyces cerevisiae. *J. Biol. Chem.*, **282**, 986–995.

51. Warren,I.A., Ciborowski,K.L., Casadei,E., Hazlerigg,D.G., Martin,S., Jordan,W.C. and Sumner,S. (2014) Extensive local gene duplication and functional divergence among paralogs in Atlantic salmon. *Genome Biol. Evol.*, **6**, 1790–1805.

52. Kenneth,H.W. and Denis,C.S. (1997) Molecular evidence for an ancient duplication of the entire yeast genome. *Nature*, **387**, 708–713.

53. Dietrich,F., Voegeli,S., Brachat,S., Lerch,A., Gates,K., Steiner,S., Mohr,C., Pöhlmann,R., Luedi,P., Choi,S. *et al.* (2004) The Ashbya gossypii genome as a tool for mapping the ancient Saccharomyces cerevisiae genome. *Science*, **304**, 304–307.